

Article

Hairy Gels: A Computational Study

Filip Uhlik ^{1,*}, Oleg V. Rud ^{1,2,*} , Oleg V. Borisov ^{2,3,*} and Ekaterina B. Zhulina ^{2,*} 

¹ Department of Physical and Macromolecular Chemistry, Faculty of Science, Charles University, 128 00 Prague, Czech Republic

² Institute of Macromolecular Compounds of the Russian Academy of Sciences, 199004 St. Petersburg, Russia

³ Institut des Sciences Analytiques et de Physico-Chimie Pour l'Environnement et les Matériaux, UMR 5254 CNRS UPPA, CEDEX 9, 64053 Pau, France

* Correspondence: uhlik@sals.natur.cuni.cz (F.U.); oleg.rud@natur.cuni.cz (O.V.R.); oleg.borisov@univ-pau.fr (O.V.B.); kzhulina@hotmail.com (E.B.Z.)

Abstract: We present results of MD and MC simulations of the equilibrium properties of swelling gels with comb-like or bottlebrush subchains and compare them to scaling-theory predictions. In accordance with theory, the simulation results demonstrate that swelling coefficient of the gel increases as a function of the polymerization degree of the main chains and exhibits a very weak maximum (or is virtually constant) as a function of the polymerization degree and grafting density of side chains. The bulk osmotic modulus passes through a shallow minimum as the polymerization degree of the side chains increases. This minimum is attributed to the onset of overlap of side chains belonging to different bottlebrush strands in the swollen gel.

Keywords: gels; bottlebrush; scaling theory; Monte Carlo; molecular dynamics



Citation: Uhlik, F.; Rud, O.V.; Borisov, O.V.; Zhulina, E.B. Hairy Gels: A Computational Study. *Gels* **2022**, *8*, 793. <https://doi.org/10.3390/gels8120793>

Academic Editors: Aleksander Czekanski and Cuiying Jian

Received: 7 November 2022

Accepted: 29 November 2022

Published: 3 December 2022

Publisher's Note: MDPI stays neutral with regard to jurisdictional claims in published maps and institutional affiliations.



Copyright: © 2022 by the authors. Licensee MDPI, Basel, Switzerland. This article is an open access article distributed under the terms and conditions of the Creative Commons Attribution (CC BY) license (<https://creativecommons.org/licenses/by/4.0/>).

1. Introduction

Brush-like macromolecules (molecular brushes) have been extensively studied theoretically and experimentally for a number of decades [1–11]. Both intra- and intermolecular interactions between side chains densely attached to the molecular backbone determine specific conformational and dynamic properties of molecular brushes, as compared to linear analogues. Chemical (covalent) cross-linking of brush-like polymers with subsequent swelling in a good solvent gives rise to the so called “hairy” gels with strands constituted by molecular brushes. The swelling ratios and osmotic moduli of such gels depend in a complex way on the grafting density and polymerization degree of the side chains decorating the network strands [12–16]. Similar structures (“hairy mesogels”) arise upon self-assembly of triblock copolymers with a comb-like or bottlebrush central block and associated terminal blocks [12,17]. In these, physically cross-linked networks the strands are formed by central blocks of copolymer (molecular brushes) that connect neighboring domains of associated blocks (network cross-links).

A molecular brush consists of a linear chain backbone with multiple side chains tethered to it. Three major synthetic approaches: (i) “grafting to” (pre-synthesized side chains are covalently attached to the backbone); (ii) “grafting through” (polymerization of the so-called macromonomers), and (iii) “grafting from” (side chains are polymerized from the backbone as macroinitiator) produced a wide variety of molecular brushes with linear grafts. An additional structural complexity can be introduced through selective gradients in grafting density or block copolymers as side chains [2,18,19].

The possibility to vary architectural parameters of molecular brushes (such as side chain length and grafting density) allows for control and adjustment of static and dynamic properties of both bulk materials and gels thereof [2,6]. Furthermore, branched architectures with bottlebrush motifs, such as barbwire [20–22] or dendronized polymers [23,24], have been synthesized and explored theoretically and experimentally [25–27]. Combining branched architecture with temperature-, pH-, and light-responsive functions in the

main and side chains of molecular brushes opens new opportunities for smart material design [17,28–35]. Since properties of the constituent macromolecules play a governing role in functions of the materials, analytical theories [36–42] and self-consistent field numerical [43] approaches; and coarse-grained computer simulations [44–53] of branched polymers have been used to corroborate the relationships between macromolecular architecture and experimentally accessible properties of melts, solutions, and thin films comprising molecular brushes.

It was demonstrated [31] that thermo-responsive triblock copolymers with linear (L) terminal and bottlebrush (B) central blocks can produce hydrogels upon association of L-blocks in spherical domains physically cross-linking B-strands. For example, PNIPAM-bbPEG-PNIPAM triblocks self-assembled upon reaching their lower critical solution temperature (LCST) to produce two types of polymer networks: injectable hydrogels at body temperature and elastomers after water evaporation [31]. The gelation process was attributed to LCST-triggered microphase separation of the PNIPAM L-blocks, and the forming network in both hydrogels and elastomers was homogeneous, in contrast to microphase-separated linear counterparts.

Self-assembly of bottlebrush block copolymers in solutions remains a topic of intensive experimental [54–64] and theoretical [42,65,66] research. It was demonstrated that branched architecture of soluble blocks leads to a variety of self-assembling aggregates that could potentially serve as precursors of gels with bottlebrush strands.

The goal of this paper is to compare the recent theoretical predictions on “hairy” gels with the results of MD and MC computer simulations. In Section 2, we briefly review the scaling model of hairy gels, and summarize the theoretical predictions on its swelling behavior and mechanical properties. We then compare the theoretical predictions with the data from Monte Carlo (MC) and molecular dynamic (MD) simulations. In Section 4, we present the details of implemented MC and MD methods. In Section 3, we formulate conclusions and outline perspectives for further development in theory and modeling of bottlebrush architectures.

2. Results and Discussion

2.1. “Hairy” Polymer Gel: Scaling Model

Swelling of chemically and/or physically cross-linked networks with brush-like strands in a good solvent yields “hairy” gels. Each strand in a hairy gel constitutes a molecular brush with degree of polymerization (DP) M in its flexible backbone (main chain), and equally flexible spacers and side chains with DPs m and n , respectively (see Figure 1a). In contrast to networks with linear strands, the swelling and elastic properties of hairy gels depend not only on the cross-linking density defined by the strand DP $N = M(1 + n/m)$, but also on n and grafting density ($1/m$) of side chains at a given M . If $n > m$, side chains overlap and stretch normally to the backbone due to monomer–monomer interactions, giving rise to a bottlebrush (molecular brush). If $n < m$, the side chains exhibit coil conformations, making the polymer comb-like.

A molecular brush is envisioned as a wormlike chain with thickness D (which is end-to-end distance of the side chains normally to the backbone), spacer end-to-end distance h , effective contour length $L \cong Mh/m$, and persistence length $l_p \simeq D$. In the framework of scaling model [36,42], the strand thickness D and spacer end-to-end distance h are specified by the balance between the elastic stretching of side chains and spacers, and repulsive monomer–monomer interactions in the cylindrical layer around the main chain, to give

$$D/a \cong \begin{cases} n^{\nu}(n/m)^{\nu(1-\nu)/2}, & m \geq m^* \\ n^{2\nu/(1+\nu)}m^{-(1-\nu)/(1+\nu)}, & m \leq m^* \end{cases} \quad (1)$$

$$h/a \cong \begin{cases} m^{\nu}(n/m)^{\nu(1-\nu)/2}, & m \geq m^* \\ m, & m \leq m^* \end{cases} \quad (2)$$

The first and the second lines in Equations (1) and (2) correspond to partial and close to maximal stretching of spacers in the main chain, respectively (with $m^* \cong n^{\nu/(2+\nu)}$ separating two elasticity regimes for the backbone); a is the length of monomer unit in the backbone and side chain; and ν is Flory exponent ($\nu \approx 3/5$ in good solvent, and $\nu = 1/2$ in theta-solvent). Notably, the scaling relations in Equations (1) and (2) have asymptotic character—that is, they apply only for $n \gg 1$, $n \gg m$, and $M \gg M^*$ with

$$M^* \simeq \begin{cases} m^{1-\nu} n^\nu, & m \geq m^* \\ n^{2\nu/(1+\nu)} m^{-(1-\nu)/(1+\nu)}, & m \leq m^* \end{cases}$$

In scaling terms, $M \simeq M^*$ (or, equivalently $L \simeq D$) separates bottlebrushes with $L \gg D$ from starlike polymers with $L \ll D$. In realistic experimental and simulation systems, $n \leq 10^2$ and $m \simeq 1$. Due to the local cylindrical symmetry, a strong overlap of moderately long side chains occurs only close to the backbone, and therefore the scaling dependences predicted by Equations (1) and (2) are only approached in the currently attainable range of n , m , and M . However, due to still noticeable stretching of the side chains normally to the backbone ($D > an^\nu$), a bottlebrush molecule behaves as a self-avoiding chain composed of L/D impermeable subunits (“superblobs” with size D each), and its overall size R_{eq} in dilute solution scales as

$$R_{eq} \cong D \left(\frac{L}{D}\right)^{3/5} = \left(\frac{Mh}{ma}\right)^{3/5} \left(\frac{D}{a}\right)^{2/5} \tag{3}$$

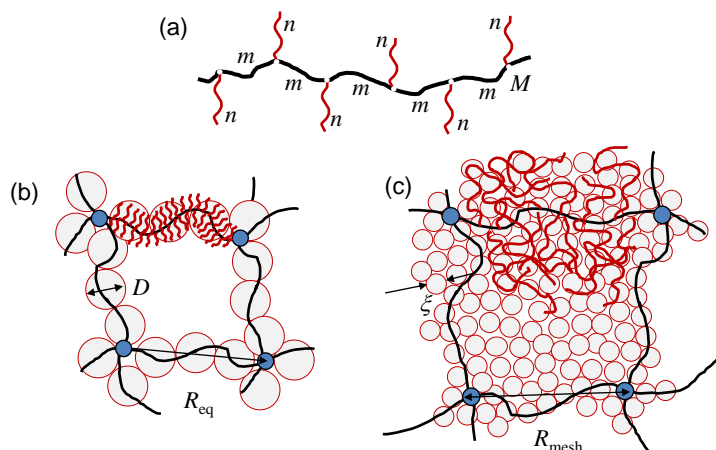


Figure 1. Schematics of graft-polymer, with $\{M, n, m\}$ being the DPs of the main and side chains and of the spacers, respectively. (a) Hairy gel with bottlebrush strands in hollow mesh (b) and filled mesh (c) regimes. Backbones of strands are colored in black, side chains are in red, and cross-links are marked as blue circles. R_{eq} is the equilibrium end-to-end distance of the main chains of the gel strands (the mesh size). Superblobs with size D (hollow-mesh regime) and concentration blobs with size $\xi < D$ in semi-dilute solution of side chains (filled-mesh regime) are shaded light gray.

Distribution of polymer’s density within a swollen hairy gel could be inhomogeneous. Two structural regimes, hollow mesh and filled mesh gel, are distinguished depending on the ratio between the mesh size, R_{mesh} , and the superblob size, D [15,16]. In the hollow mesh regime (Figure 1b), each strand constitutes a molecular brush with thickness $D \ll R_{mesh}$, and weak overlap of neighboring strands ensures hollow space (mesh) between cross-links. In this case, the mesh size R_{mesh} can be evaluated using the c^* -theorem of de Gennes, [67] to give $R_{mesh} \simeq R_{eq}$. In the filled-mesh regime (Figure 1c), the neighboring strands strongly overlap, giving rise to a semi-dilute solution of side chains with an almost uniform concentration $c \simeq Na^3/R_{mesh}^3$. The interior of the gel is envisioned as a closely-packed array of the concentration blobs with size $\xi(c) \sim ac^{-\nu/(3\nu-1)} < D$. In this case, the equilibrium mesh size R_{mesh} results from the balance between gel osmotic pres-

sure, $\pi/k_B T \cong \zeta^{-3}(c)$, and the conformational elasticity of the backbones (renormalized according to the polymer concentration c inside the gel).

To facilitate comparison between the theoretical predictions and the simulation data, we present in Figure 2 the scaling-type diagram of states for hairy gels [16] in n, m log–log coordinates (with $\nu = 3/5$). In the hollow-mesh regimes C_a^* and C_b^* , each spacer in the main chain is, respectively, partially or almost fully stretched. The boundary $C_a^* - C_b^*$ corresponds thereby to $m = m^*$, indicating the onset of spacer strong stretching in individual strands at given n . Similar situation occurs in the filled mesh regimes C_a^{**} and C_b^{**} . That is, the boundary $C_a^{**} - C_b^{**}$ corresponds to the onset of spacer strong stretching in the filled-mesh regimes (semi-dilute solutions of the side chains). At the boundaries $C_b^* - C_b^{**}$ and $C_a^* - C_a^{**}$ (red lines in Figure 2), DP M of the backbone becomes equal (in scaling terms) to M^* , separating bottlebrush and starlike conformations of strands. At these boundaries (indicated by M^*), each strand comprises on the order of one superblob with size D ($L \simeq D$), as schematically shown in Figure 2.

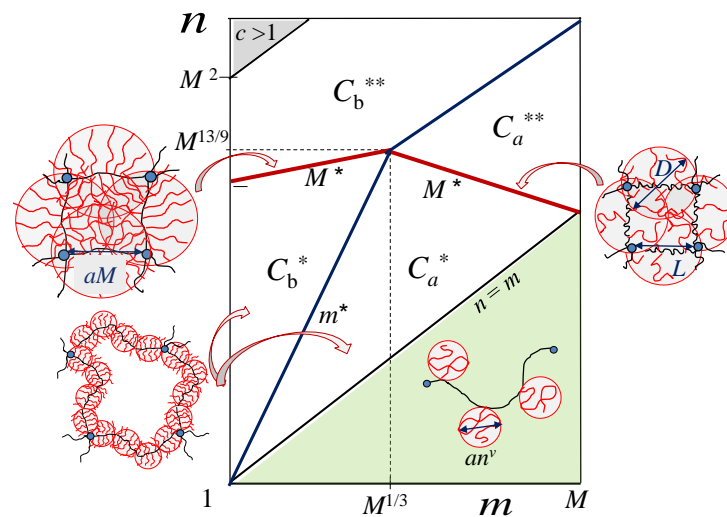


Figure 2. Scaling-type diagram of states for hairy gel in $\{n, m\}$ coordinates in good solvent ($\nu = 3/5$). In the hollow-mesh regimes C_b^* and C_a^* , bottlebrush strands have either partially or almost fully stretched spacers, respectively. In filled-mesh regimes C_b^{**} and C_a^{**} , the interior of the gel constitutes a semi-dilute solution of side chains. Schematics demonstrate strand conformations in regimes C_b^* and C_a^* , and at boundaries $C_b^* - C_b^{**}$ and $C_a^* - C_a^{**}$ (that correspond to backbone length $M = M^*$ at which bottlebrush transforms in starlike polymer with $L = D$). Boundary $C_b^* - C_a^*$ (marked m^*) separates bottlebrush strands with fully ($m < m^*$) and partially ($m > m^*$) stretched spacers. In the shaded green area, strands are comb-like (side chains are unstretched coils). Strands in regimes of semi-dilute solutions C_b^{**} and C_a^{**} are shown in Figure 1.

The scaling expressions for the equilibrium mesh size R_{mesh}/aM^ν , gel swelling coefficient (that is, ratio of volumes V in the swollen and dry states)

$$Q = \frac{V}{V_{dry}} \simeq \frac{R_{mesh}^3}{a^3 N} = \frac{R_{mesh}^3}{a^3 M} \cdot \left(\frac{m}{n}\right), \tag{4}$$

with $N = M(1 + n/m)$ and $n \gg m$, and osmotic bulk modulus

$$\frac{G}{k_B T} = c \left(\frac{\partial \pi}{\partial c} \right)_{c=c_{eq}} \simeq \begin{cases} R_{mesh}^{-3} & \text{hollow mesh regimes } C_a^*, C_b^* \\ \zeta(c)^{-3} & \text{filled mesh regimes } C_a^{**}, C_b^{**} \end{cases} \tag{5}$$

are collected in Table 1 with corresponding exponents specified for $\nu = 3/5$.

Table 1. Asymptotic power-law dependencies for normalized mesh size R_{mesh} , swelling ratio Q , and bulk osmotic modulus G in a free-swelling hairy gel with DP M of strands in good solvent ($\nu = 3/5$).

	$R_{mesh}/aM^{3/5}$	$QM^{-4/5}$	$Ga^3M^{9/5}/k_B T$
C_a^*	$(n/m)^{9/25}$	$(n/m)^{2/25}$	$(n/m)^{-27/25}$
C_a^{**}	$(n/m)^{9/25}$	$(n/m)^{2/25}$	$(n/m)^{-9/50}$
C_b^*	$(n/m)^{3/10}m^{1/5}$	$(n/m)^{-1/10}m^{3/5}$	$(n/m)^{-9/10}m^{-3/5}$
C_b^{**}	$M^{2/5}$	$M^{6/5}(n/m)^{-1}$	$M^{-27/10}(n/m)^{9/4}$

As follows from Table 1, an increase in DP n of the side chains at fixed DP M of the backbone leads to the monotonous increase in mesh size, $R_{mesh} \sim n^\beta$, in regimes C_a^* and C_a^{**} (exponent $\beta = 9/25 = 0.36$), C_b^* (exponent $\beta = 3/10$), approaching full extension, $R_{mesh} \sim aM$, in regime C_b^{**} (exponent $\beta = 0$). At the same time, both swelling ratio Q and osmotic bulk modulus G exhibit non-monotonic dependences on n . Swelling coefficient $Q(n) \sim n^{3\beta-1}$ passes through a maximum at the boundaries $C_a^* - C_b^*$ and $C_a^{**} - C_b^{**}$, and osmotic modulus $G(n)$ passes through a minimum upon crossing the boundaries of regime C_b^{**} . The maximum in $Q(n)$ dependence is weak due to a small value of the exponent which changes from $+0.08$ to -0.1 at the $C_a^* - C_b^*$ boundary, and this maximum could even disappear if the apparent exponent $\beta_{app} < 1/3$. Recall that the values of exponents in Table 1 were calculated in the limit of $n/m \gg 1$. The predicted sharp (jumpwise) minimum in $G(n)$ at the boundaries of regime C_b^{**} could be smoothed in computer simulations, leading to shift in the minimum location far left (to smaller values of n).

2.2. Computer Simulations of Hairy Gel

We used both MC and MD simulations to explore the equilibrium-swelling behavior of hairy gels in a good solvent ($\nu = 3/5$). In Figure 3, we present the simulation box which has the same geometry in MC and MD simulations. That is, 16 polymer chains were connected to a diamond-like network by eight tetrafunctional cross-linking units, and the network element was put into cubic simulation box of the volume V with periodic boundary conditions to emulate an infinite polymer network. It is worth mentioning that MD and MC simulations were performed in NVT and NPT (with pressure $P = 0$ and V fluctuating) ensembles, respectively.

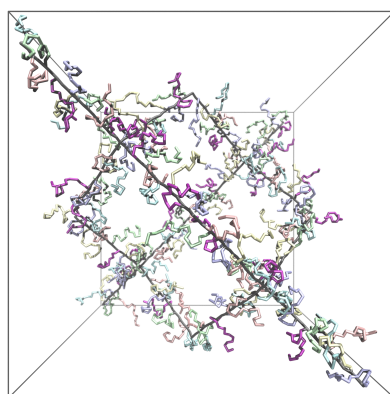


Figure 3. A view of a simulation unit cell with gel backbone (in black color, length $M = 19$) and side chains (in various light colors for clarity, length $n = 16$) grafted every second monomer unit ($m = 2$) intentionally in a state with pressure $P < 0$ (volume V greater than in free swelling equilibrium with pressure $P = 0$) to avoid excessive overlapping of side-chains and clearly showing the gel branching. Backbones are indicated in black with side chains in various colors (to avoid crowding).

In Figure 4a,b, we present the scaling-type diagrams with positions of the boundaries calculated specifically for DP $M = 37$ and DP $M = 13$ of the backbone, respectively,

together with set of symbols $\{n, m\}$ marking the architectural parameters of bottlebrush strands modeled in MC simulations. In Figure 4c, a similar diagram is presented for $M = 30$ with set of symbols $\{n, m\}$ marking the parameters of strands modeled in MD simulations.

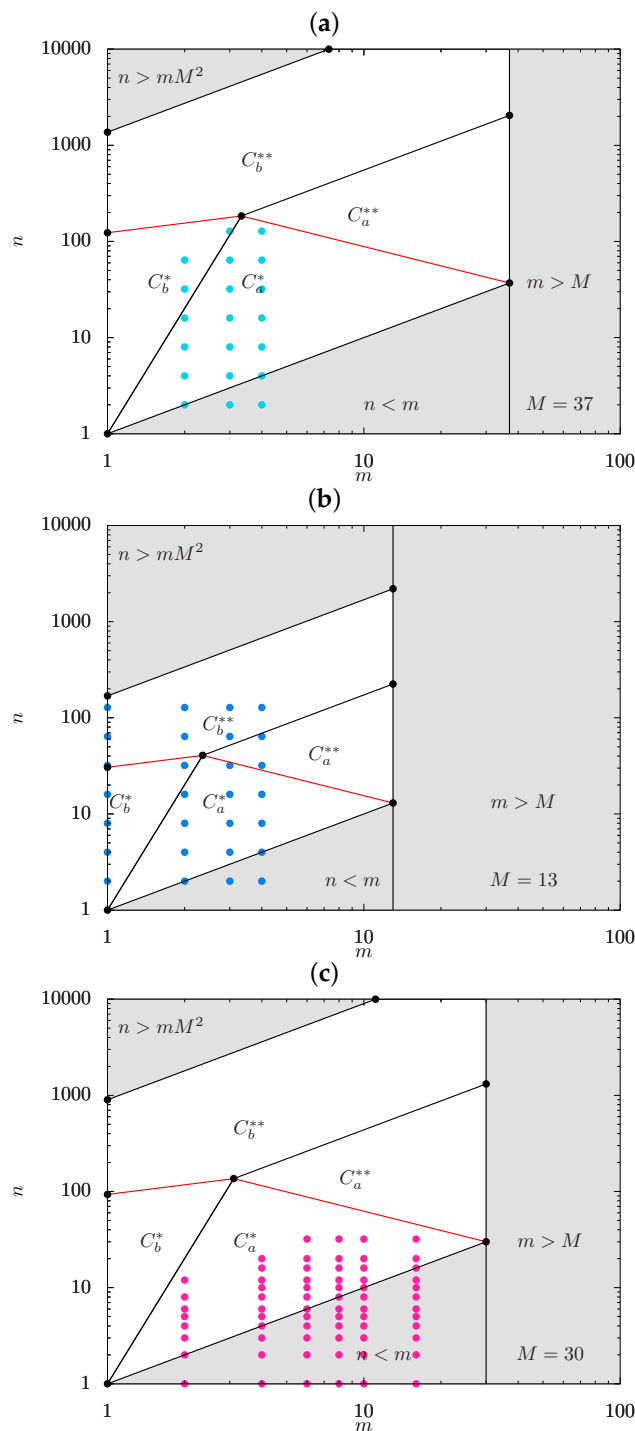


Figure 4. Scaling-type diagrams with positions of boundaries calculated specifically for DP $M = 37$ (a) and DP $M = 13$ (b) of the backbone, respectively, together with ordered set of symbols $\{n, m\}$ marking the architectural parameters of bottlebrush strands modeled in MC simulations and (c) for $M = 30$ in MD simulations. Shaded area with $n \geq mM^2$ corresponds to unphysical values of $c \geq 1$.

While positions of the boundaries in Figure 4 are specified with accuracy of the numerical prefactors on the order of unity, it is still expected that MC simulations for $M = 37$ (Figure 4a) with small values of $1 \leq m \leq 4$ and increasing n (up to $n = 128$) cover

regimes C_a^* and C_b^* . In contrast, Figure 4b indicates that for $M = 13$, MC data pass through regimes C_a^* C_b^* , and even enters regime C_b^{**} . According to Figure 4c, MD simulations cover a considerably larger interval of m -values (up to $m = 50$). However, many of the symbols correspond to comb-like strands (area with $n/m < 1$, shaded gray), and the rest of the data probes only regime C_a^* .

2.2.1. Average End-to-End Distances of Strands and Side Chains

In Figures 5, we plot the average mesh size $R_{mesh} \simeq \langle V \rangle^{1/3}$ of a free-swelling gel, and the average end-to-end distance $\langle r \rangle \simeq r_{sc} \simeq D$ of the side chains obtained in MC simulations as a function of n for $m = 1, 2, 3$, and 4 in log–log coordinates.

At $n \gtrsim 10$ (when the side chains stretch normally to the backbone), different m -values produce almost parallel lines in $R_{mesh}(n) \sim n^\beta$ dependences, with apparent slopes $\beta_{app} = 0.22 - 0.25$, i.e., smaller than the theoretically predicted β (i.e., 0.36 in regime C_a^* and 0.30 in regime C_b^*). For $r_{sc}(n) \sim n^\alpha$, the correspondence between the theoretical exponents α (i.e., 0.75 in regimes C_b^* and 0.72 in regime C_a^*) and apparent slopes is expectably [50] worse, consistent with smaller apparent values of β_{app} . Notably, at $M = 37$, $R_{mesh}(n)$, and $r_{sc}(n)$ do not intersect at fixed m at any considered n (see Figure 5a), indicating that the hairy gel remains in the hollow mesh state. In contrast, at $M = 13$, $R_{mesh}(n)$ and $r_{sc}(n)$ become close at the largest values of n (see Figure 5b), indicating that the hairy gel approaches the filled-mesh state. In Figure 5c, we plot normalized mesh size $R_{mesh}/aM^{3/5}$ as a function of (n/m) for $M = 13, 19, 25$, and 37 to demonstrate how MC data collapse on mastercurve with slope $\beta_{app} = 0.25$, with maximal deviations for the smallest value of $M = 13$ (presumably approaching regime C_b^{**} with $R_{mesh}/aM^{3/5} \sim (n/m)^0$).

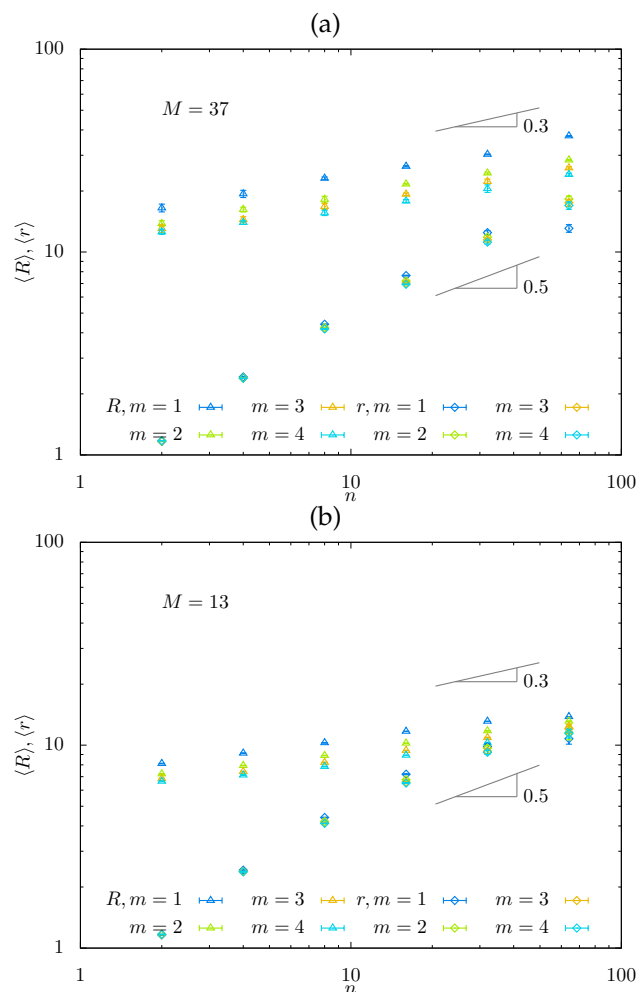


Figure 5. Cont.

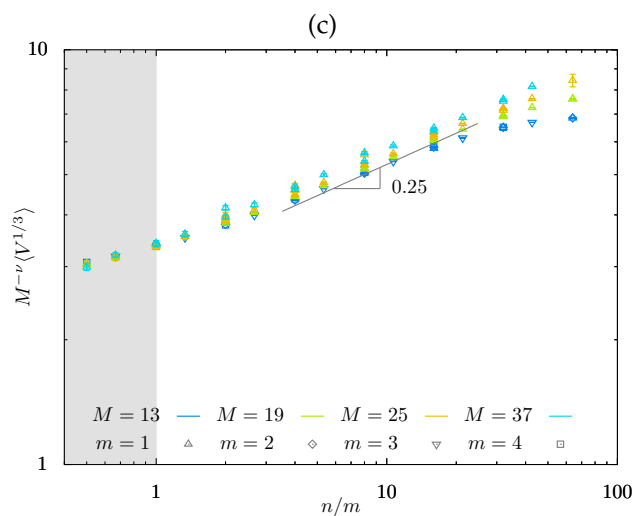


Figure 5. Average mesh size $R = \langle V \rangle^{1/3}$ and end-to-end distances of the side chains $\langle r \rangle$ as a function of n for $m = 1, 2, 3, 4$ for $M = 13$ (a) and $M = 37$ (b) obtained from MC simulations. In panel (c), the mesh size is normalized by M^ν . Here and below, the gray area corresponds to comb-like strands with $n/m < 1$.

In Figure 6, the equilibrium strand end-to-end distance $R_{mesh}(n) \sim \langle V \rangle^{1/3}$ is presented for a series of m -values and fixed $M = 30$, as obtained from MD simulations. While values of $n < m$ correspond to comb-like strands, the data for relatively small m and $n > 10$ are used in Figure 6 to evaluate apparent exponent β_{app} in the dependence $R_{mesh}(n)M^{-3/5} \sim (n/m)^{\beta_{app}}$ to give $\beta_{app} \approx 0.26$, in accordance with the results of MC simulations.

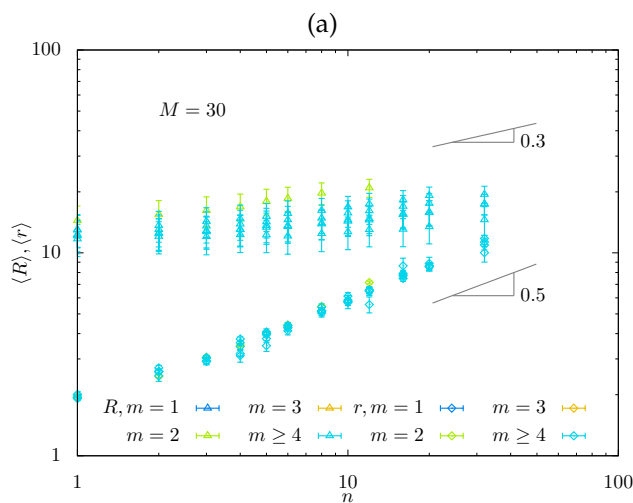


Figure 6. Cont.

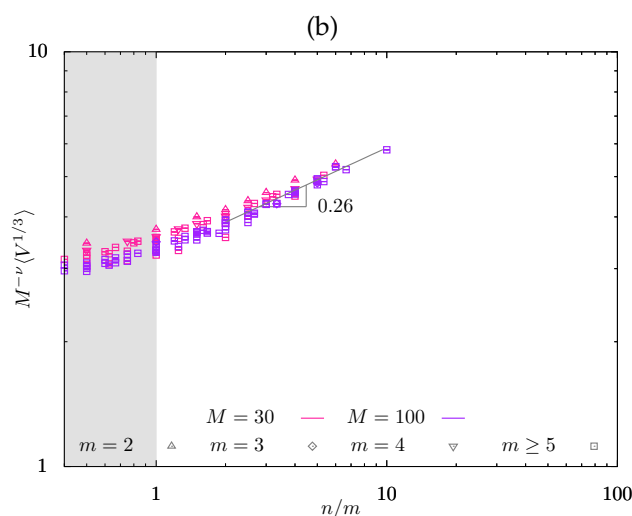


Figure 6. Equilibrium mesh size from MD simulations, $R_{mesh}(n) \sim V^{1/3}$, as a function of n for a series of m -values and fixed $M = 30$ (a), and normalized mesh size $R_{mesh}(n)M^{-3/5}$ versus n/m with slope $\beta_{app} = 0.26$ (b).

2.2.2. Gel Swelling Coefficient

In Figure 7, we present the normalized equilibrium swelling coefficient $QM^{-4/5} = VM^{-4/5}/a^3N$ as a function of n/m predicted by the scaling model (Figure 7a) and obtained from MC simulations (Figure 7b) in log–log coordinates. The power-law dependences $QM^{-4/5}$ in Figure 7a were calculated for $M = 37$ with slopes indicated in Table 1 (that is, $2/25$, $-1/10$, and -1 in regimes C_a^* , C_b^* , C_b^{**} , respectively) and $m = 1, 2, 3$, with all numerical prefactors assigned unity. For $m = 2$, Q is shown by red lines; for $m \geq 4$ only regimes C_a^* , C_b^{**} are feasible. The maximum predicted for $M = 37$ corresponds to $QM^{-4/5} \approx 1.38$. A decrease in M shifts location of the maximum to the left and makes it less pronounced.

MC simulations data in Figure 7b show the dependence of $QM^{-4/5}$ on n/m for series of M -values. The predicted weak maximum is not well pronounced; mostly, its decreasing (right) branch is seen in MC simulations. As strands with $M = 37$ are not expected to enter regime C_b^{**} (see Figure 4a), the slope dQ/dn is far from the predicted exponent -1 . However, for smaller $M = 13$ for which regime C_b^{**} is feasible (see Figure 4b), the slope of MC data approaches -1 , as predicted.

The data from MD simulations in Figure 8 also indicate weak dependence of swelling coefficient Q on n/m . Here, the normalized swelling coefficient $QM^{-4/5}$ is presented as a function of n/m for a wider variety of m -values and two values of $M = 30$ (red symbols) and $M = 100$ (violet symbols), and probing regime C_a^* in which the predicted slope is $2/25 = 0.08$. For $M = 30$, the data in Figure 8 with different m -values remain rather scattered; the increase in backbone DP M up to $M = 100$ decreases the scattering of the data that collapse on mastercurve with close to zero slope. Notably, the numerical prefactor in $QM^{-4/5}$ versus n/m dependences is close to unity in both MC and MD simulations, consistent with the scaling model.

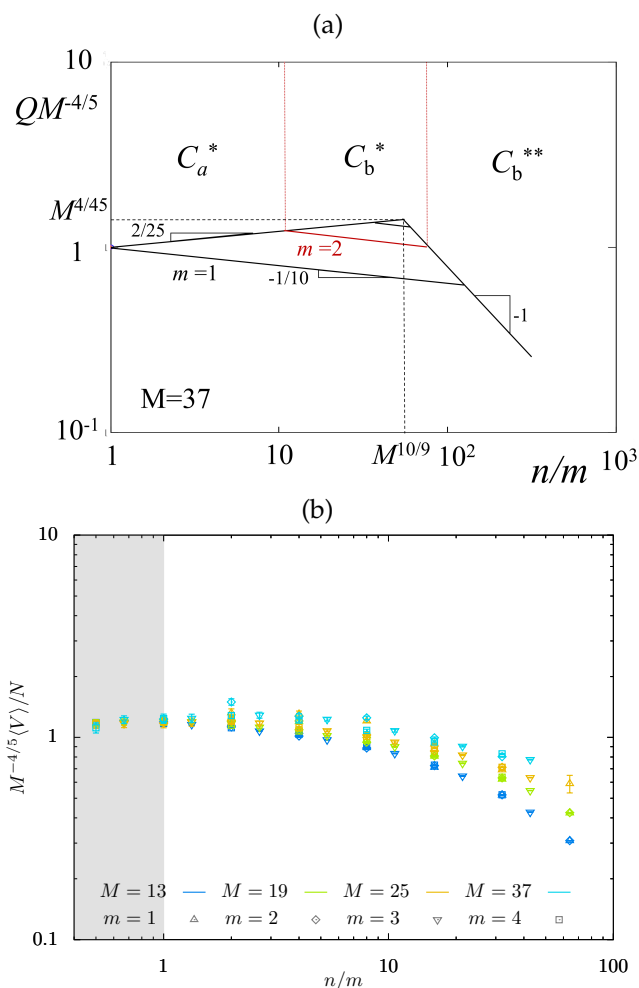


Figure 7. Theoretical (a) and MC-simulated (b) swelling coefficient Q as a function of n/m . Scaling dependences for theoretical Q (with all numerical coefficients equal to unity) were calculated for $M = 37$. $C_a^* - C_b^*$ and $C_b^* - C_b^{**}$ boundaries are indicated for $m = 2$.

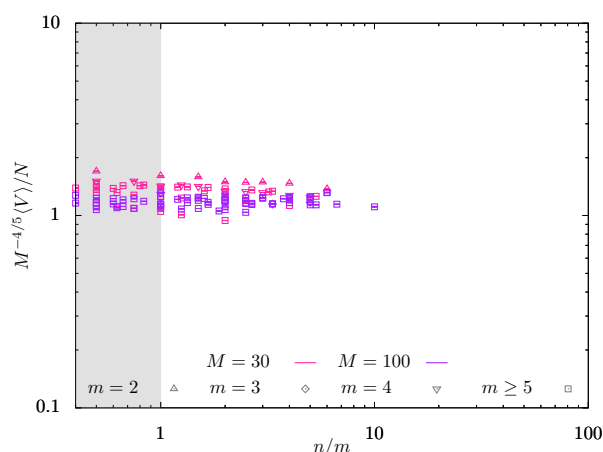


Figure 8. Normalized swelling coefficient $QM^{-4/5}$ from MD simulations for $M = 30$ (red symbols) and 100 (violet symbols) as a function of n/m .

2.2.3. Osmotic Bulk Modulus

In Figure 9a we present the MC data for the gel osmotic bulk modulus, $G = c(\partial\pi/\partial c)_{c=c_{eq}}$. Here, $\pi(c)$ is osmotic pressure, and $c_{eq} \simeq Q^{-1}$ is the equilibrium concentration of monomer units in the hairy gel. As is seen in Figure 9a, the osmotic modulus G decreases with

increasing DP M of the strand backbone, in qualitative agreement with the theoretical predictions in Table 1. However, the predicted minimum in $G(n)$ dependence is not detected in MC simulations. An increase in M flattens $G(n)$ dependence, only pointing at the possibility of minimum formation.

A conjecture is that the sharp minimum predicted by the scaling model could be smoothed in MC simulations, as schematically illustrated by the dashed lines in Figure 9b. Another factor is the effect of perturbed dense cylindrical layers circumventing the backbones. Although Figure 9b is merely schematic and does not specify the shape or position of the dotted lines, it is clear that the theoretically predicted exponents for $G(n)$ would not work in the smoothed region, and therefore, collapse of G -data on the mastercurve is not expected. However, this schematic indicates that minimum in $G(n)$ dependence can move left and fall out of the considered ranges of the strand architectural parameters.

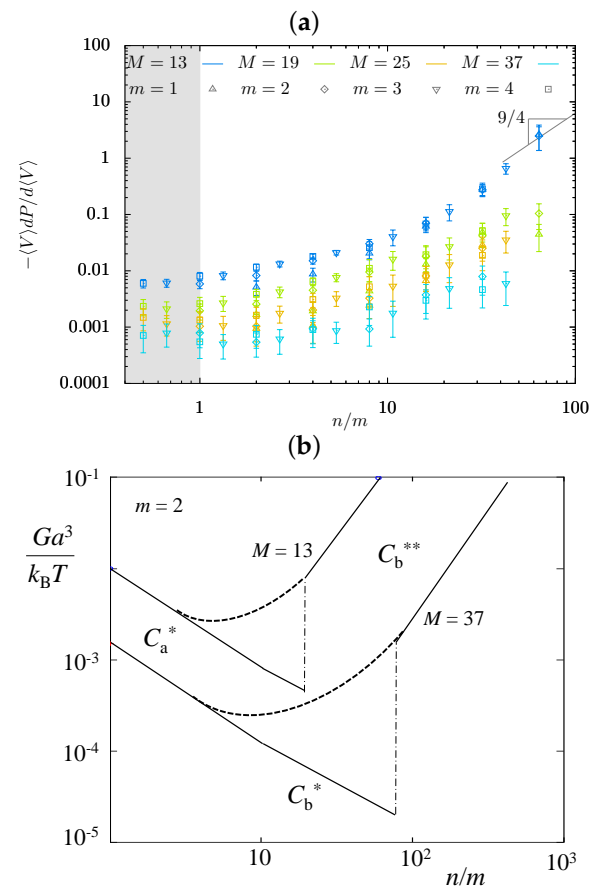


Figure 9. Osmotic modulus G as a function of n/m in MC simulations (a) and scaling model (b). A conjecture that sharp minimum could be smoothed in simulations is illustrated by the dashed lines (b).

3. Conclusions

Based on the scaling description of molecular brushes, the theory specifies power-law dependences for the equilibrium properties of “hairy” gels with bottlebrush strands. Four structural regimes of hairy gels were distinguished: two hollow-mesh regimes, C_a^* and C_b^* , with partially and almost fully stretched spacers; and two filled mesh regimes, C_a^{**} and C_b^{**} , with partially or almost fully stretched backbones embedded in a semi-dilute solution of side chains. Two supplementary computer simulation techniques, MC and MD, were used to probe the structure of free-swelling in good solvent gel with varied strand architectural parameters $\{M, n, m\}$ to corroborate the theoretical model. It was demonstrated that MC simulations of hairy gels with short spacers ($m \leq 4$) could cover regimes C_a^* and C_b^* , and approach regime C_b^{**} . MD simulations of gels with a wider variety of m -values could

probe regime C_a^* . In all cases, limited extension of the gel regimes (Figure 4) and restriction $n/m \gg 1$ make it challenging to compare the predicted asymptotic values of exponents (Table 1) with apparent exponents from MC and MD simulations. In addition, it is not surprising that apparent exponents deviate from the theoretical ones for the considered set of strand parameters $\{M, n, m\}$.

According to the scaling model, the gel mesh size $R_{mesh} \sim M^\nu n^\beta$ increases monotonously with increasing of both the DP n of the side chain and the DP M of the strand backbone. The apparent exponent $\beta_{app} \approx 0.25 - 0.26$ estimated from MC and MD simulations was smaller but reasonably close to the theoretical values, $\beta = 0.30 - 0.36$. Exponent ν was close to $3/5$ as expected for good solvent conditions. The thickness D of the bottlebrush strand increased with n . However, an approach to the theoretical exponent $3/4$ requires $n \gtrsim 10^3$ (i.e., much larger n -values than have been implemented in MC simulations), and the correspondence between apparent and scaling exponents in $D(n)$ dependence was poor.

The theory predicts that the swelling ratio Q of the hairy gels is controlled primarily by the DP M of the strand backbone, whereas the dependence on the DP n and grafting density $1/m$ of the side chains is weak. This prediction is in agreement with the MC and MD simulation data. The theory also predicts non-monotonic dependences of osmotic modulus G and swelling ratio Q of hairy gels on DP n of the side chains. The osmotic modulus G passes through a minimum corresponding to the overlap threshold of the side chains emanating from different strands. In contrast, swelling ratio Q passes through a maximum upon onset of strong stretching of spacers in nonoverlapping strands. The MC computer simulations did not find pronounced extrema in $Q(n/m)$ and $G(n/m)$ dependences and demonstrated only the decreasing branch in Q -dependence (with slope approaching -1 , predicted in regime C_b^{**}) and the increasing branch in G -dependence (with slope approaching $9/4$, predicted in regime C_b^{**}). Lack of maximum in $Q(n)$ dependence can be explained by the values of apparent exponent $\beta_{app} < 1/3$ in $R_{mesh} \sim n^{\beta_{app}}$ dependence that automatically eliminates the increasing branch in $Q = R_{mesh}^3/a^3 N \sim n^{3\beta_{app}-1}$. The relatively small values of β_{app} could follow from the limited extension of the scaling regimes for currently considered set of $\{M, n, m\}$ parameters. A wider set of architectural parameters $\{M, n, m\}$ is desirable to confront the scaling model of hairy gel with better accuracy.

4. Materials and Methods

The model of the gel as a network of 16 linear polymer chains, each consisting of M monomer units. These polymer chains are connected to a diamond-like network by eight cross-linking units. The side chains of the length n are grafted on each m -th monomer of the main chain (see Figure 3). The network was put into cubic simulation box of the volume V_{gel} with periodic boundary conditions, which virtually emulates an infinite polymer network.

4.1. Monte Carlo Simulations

In Monte Carlo simulations, we used a variant of the Hamiltonian (originally called hybrid [68]) Monte Carlo (HMC) method and coarse-grained (CG) models. The HMC uses Hamiltonian dynamics to sample probability distribution $\exp(-H/k_B T)$, where $H(p, q)$ is the Hamiltonian, q are generalized coordinates, and p are generalized momenta. In the simplest case, a separable Hamiltonian $H(p, q) = K(q) + V(p)$ is used, where K is kinetic energy and V is potential energy for sampling Boltzmann distribution $\exp(-V(q)/k_B T)$. The momenta p can be sampled directly, and Hamiltonian dynamics $\dot{q} = \partial H / \partial p$, $\dot{p} = -\partial H / \partial q$ are followed for some time to prepare a new proposal for a Metropolis step [69] with acceptance probability $P_{acc} = \min(1, \exp(-\Delta H/k_B T))$. For the exact dynamics ΔH , it would be zero (time independent Hamiltonian is conserved), and all proposals would be accepted. In practice, instead of exact dynamics, we must use an approximate numerical evolution with numerical integrators. Fortunately, time-reversible, phase-space volume-preserving integrators are available, and their procedure is exact, and any bias due to approximate

dynamics is then removed by Metropolis rejections. Moreover, the Hamiltonian for dynamic evolution can be different from the targeted one. This allows for great variability of the method. In the case of polymer simulations, a big improvement can be achieved by a suitable transformation of variables. The potential energy for the standard Rouse (harmonic) model is diagonal in bond vector coordinates $r_i - r_{i-j}$. With the freedom of choosing the evolution Hamiltonian, we use new canonically conjugated momenta with bond vector coordinates, and it allows for sampling all normal modes at the same rate [70]. For other potentials and approximate integrators, the method somewhat deteriorates, but it is still much better than simple molecular dynamics and leads to a smaller scaling exponent of the integrated autocorrelation time of the end-to-end distance with chain length, and thus is arbitrarily faster.

In our CG model we use two types of interactions, bonding and non-bonding. For the bonding one, we use a variant of finitely extensible nonlinear elastic (FENE) potential [71] in a form $u_F(r) = -ek_B T \log((r_0 + d - x)(x - r_0 + d)/d^2)$ for $r \in (r_0 - d, r_0 + d)$ and infinite elsewhere, with mild singularities at $r_0 \pm d$. It is a relatively small complication for simple molecular dynamics where small time-steps are used that potential does not exist outside $(r_0 - d, r_0 + d)$. In HMC, we use the advantage of much longer time-steps that could lead to stepping out of the definition interval. We resolve this in the spirit of HMC and prepare a new potential finite, everywhere being $u_F(r)$ on $(r_0 - d + \epsilon, r_0 + d - \epsilon)$ and $v(r) + u(r_0 + d - \epsilon) - v(r_0 + d - \epsilon)$, where $v(r) = ek_B T (r_0/d)^2 (r/r_0 - 1)^2$ elsewhere that is used for dynamic evolution in HMC and the original $u_F(r)$ is used for the Metropolis step. By this combination, we achieve the exact sampling with $u_F(r)$ while avoiding numerical problems. For non-bonding potential, we use soft repulsive potential $u_S = e((r - c)/r)^2$ for $r \in (0, c)$ and 0 elsewhere, where $e > 0$ is an energy parameter and c is a cutoff. The potential is smooth at cutoff. Frequently, the standard Lennard–Jones potential [72], originally suggested for simulations of neon, is used for this purpose. Although the $1/r^6$ part can be justified for two atoms (with at least one in an S-state) at very long distances, the $1/r^{12}$ part lacks such a simple justification, the less for the potential that should represent CG macromolecular system in a solution. By taking a systematically coarse-grained model based on all-atom empirical force-field and fitting the corresponding part for small distances, we find a much smaller exponent [73] of about 2, as for our $u(r)$.

The simulations were performed in *NPT* ensemble by adding volume-changing moves [74]. The simulations started from extended conformations of gel backbone and coiled side-chains as corresponding to a good solvent. A thorough equilibration was performed for box sizes, energies, and end-to-end distances. The free (tuning) parameters of our HMC method were roughly set up according to optimal acceptance probability and the smallest integrated autocorrelation times. After equilibration (as illustrated by Figure 10), samples were accumulated, and standard deviations of their averages were estimated using the blocking method [75].

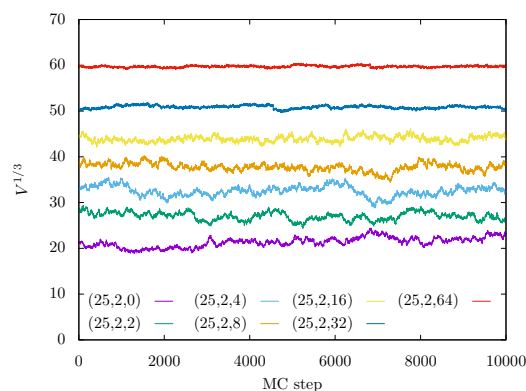


Figure 10. Traces of instantaneous box sizes during *NPT* Monte Carlo sampling for $P = 0$ and gel architectural parameters (M, m, n) , as indicated in the legend.

4.2. Molecular Dynamics Simulations

Each pair of the particles interact via the truncated Lennard–Jones interaction potential, which imposes strong repulsion between all particles at short distances:

$$U_{\text{LJ}}(r) = \begin{cases} 4\epsilon \left(\left(\frac{\sigma}{r} \right)^{12} - \left(\frac{\sigma}{r} \right)^6 \right) & \text{if } r < r_{\text{cut}} \\ 0 & \text{elsewhere} \end{cases}, \quad (6)$$

where r is the interparticle distance, $\sigma = 0.35$ nm is a chosen characteristic size of the particles, $\epsilon = k_B T$ is the depth of the potential, and r_{cut} is the cut-off distance beyond which the potential is set zero.

The bonds connecting the gel to a network are modeled using finite extension nonlinear elastic potential (FENE):

$$U_{\text{FENE}}(r) = -\frac{1}{2} K \Delta r_{\text{max}}^2 \ln \left[1 - \left(\frac{r - r_0}{\Delta r_{\text{max}}} \right)^2 \right], \quad (7)$$

where r is the distance between the bonded segments, K is the magnitude of their interaction, Δr_{max} is the maximal stretching length of the bond, and r_0 is the equilibrium bond length. In our simulations we set $K = 10kT/\sigma^2$, $\Delta r_{\text{max}} = 3\sigma$ and $r_0 = 0.0$ [76].

The Langevin thermostat [71] was used to guarantee the constant temperature of the system, $T = 300$ K. The two additional terms to force in equation of motion were added.

$$\mathbf{f}_i = -\gamma \mathbf{v}_i(t) + \sqrt{2\gamma kT} \boldsymbol{\eta}_i(t), \quad (8)$$

where the first term corresponds to constant friction, with γ being a friction coefficient, and the second one corresponds to random thermal force, with $\boldsymbol{\eta}_i$ being a normally distributed random vector; \mathbf{v}_i —velocity of i -th particle, t —time.

In order to calculate the swelling ratio of hydrogel, we performed a series of simulations of the gel in a box of different volumes V . Each simulation results in a particular value of pressure P .

Our target observable is the free swelling equilibrium state, i.e., at the state where the applied to the gel pressure equals to zero. In order to localize this state, we first plotted $P(V)$ dependence; then, using the least-squares method, we drew a line passing through the nearest to the V axis points. The place where this line crosses the V -axis defines the volume of free swelling equilibrium state.

Author Contributions: Scaling theory O.V.B. and E.B.Z.; MC simulations F.U.; MD simulations O.V.R.; writing all authors. All authors have read and agreed to the published version of the manuscript.

Funding: This work was supported by Russian Science Foundation, grant 20-13-00270.

Institutional Review Board Statement: Not applicable.

Conflicts of Interest: There are no conflict of interest to declare.

References

1. Sheiko, S.S.; Sumerlin, B.S.; Matyjaszewski, K. Cylindrical molecular brushes: Synthesis, characterization and properties. *Prog. Polym. Sci.* **2008**, *33*, 759–785. [[CrossRef](#)]
2. Verduzco, R.; Li, X.; Pesek, S.L.; Stein, G.E. Structure, function, self-assembly of bottlebrush copolymers. *Chem. Soc. Rev.* **2015**, *44*, 2405–2420. [[CrossRef](#)] [[PubMed](#)]
3. Müllner, M.; Müller, A.H.E. Cylindrical polymer brushes—Anisotropic building blocks, unimolecular templates and particulate nanocarriers. *Polymer* **2016**, *98*, 389–401. [[CrossRef](#)]
4. Rzayev, J. Molecular Bottlebrushes: New Opportunities in Nanomaterials Fabrication. *ACS Macro Lett.* **2012**, *1*, 1146–1149. [[CrossRef](#)] [[PubMed](#)]

5. Li, X.; Prukop, S.L.; Biswal, S.L.; Verduzco, R. Surface Properties of Bottlebrush Polymer Thin Films. *Macromolecules* **2012**, *45*, 7118–7127. [[CrossRef](#)]
6. Liang, H.; Sheiko, S.S.; Dobrynin, A.V. Supersoft Polymer Networks with Brushlike Strands. *Macromolecules* **2018**, *51*, 638–645. [[CrossRef](#)]
7. Yuan, J.; Müller, A.H.E.; Matyjaszewski, K.; Sheiko, S. *Polymer Science: A Comprehensive Reference*; Matyjaszewski, K., Möller, M., Eds.; Elsevier: Amsterdam, The Netherlands, 2012.
8. Clair, C.; Lallam, A.; Rosenthal, M.; Sztucki, M.; Vatankhah-Varnosfaderani, M.; Keith, A.N.; Cong, Y.; Liang, H.; Dobrynin, A.V.; Sheiko, S.S.; et al. Strained Bottlebrushes in Super-Soft Physical Networks. *ACS Macro Lett.* **2019**, *8*, 530–534. [[CrossRef](#)]
9. Xie, G.; Martinez, M.R.; Olszewski, M.; Sheiko, S.S.; Matyjaszewski, K. Molecular Bottlebrushes as Novel Materials. *Biomacromolecules* **2019**, *20*, 27–54. [[CrossRef](#)]
10. Rathgeber, S.; Pakula, T.; Wilk, A.; Matyjaszewski, K.; Beers, K.L. On the shape of bottle-brush macromolecules: Systematic variation of architectural parameters. *J. Chem. Phys.* **2005**, *122*, 124904. [[CrossRef](#)]
11. Li, Z.; Tang, M.; Liang, S.; Zhang, M.; Biesold, G.M.; He, Y.; Hao, S.-M.; Choi, W.; Liu, Y.; Peng, J.; et al. Bottlebrush polymers: From controlled synthesis, self-assembly, properties to applications. *Prog. Polym. Sci.* **2021**, *116*, 101397. [[CrossRef](#)]
12. Li, T.; Huang, F.; Diaz-Dussan, D.; Zhao, J.; Srinivas, S.; Narain, R.; Tian, W.; Hao, X. Preparation and Characterization of Thermoresponsive PEG-Based Injectable Hydrogels and Their Application for 3D Cell Culture. *Biomacromolecules* **2020**, *21*, 1254–1263. [[CrossRef](#)] [[PubMed](#)]
13. Sarapas, J.M.; Chan, E.P.; Rettner, E.M.; Beers, K.L. Compressing and Swelling To Study the Structure of Extremely Soft Bottlebrush Networks Prepared by ROMP. *Macromolecules* **2018**, *51*, 2359–2366. [[CrossRef](#)]
14. Sheiko, S.S.; Vashahi, F.; Morgan, B.J.; Maw, M.; Dashtimoghadam, E.; Fahimipour, F.; Jacobs, M.; Keith, A.N.; Vatankhah-Varnosfaderani, M.; Dobrynin, A.V. Mechanically Diverse Gels with Equal Solvent Content. *ACS Cent. Sci.* **2022**, *8*, 845–852 [[CrossRef](#)]
15. Zhulina E.B.; Sheiko S.S. Borisov, O.V. Polymer Networks Formed by Molecular Brushes: Scaling Theory. *Polym. Sci. Ser. A* **2019**, *61*, 799–804. [[CrossRef](#)]
16. Zhulina, E.B.; Borisov, O.V. Bottlebrush polymer gels: Architectural control over swelling and elastic moduli. *Soft Matter* **2022**, *18*, 1239–1246. [[CrossRef](#)]
17. Jacobs, M.; Liang, H.; Dashtimoghadam, E.; Morgan, B.J.; Sheiko, S.S.; Dobrynin, A.V. Nonlinear Elasticity and Swelling of Comb and Bottlebrush Networks. *Macromolecules* **2019**, *52*, 5095–5101. [[CrossRef](#)]
18. Kerr, A.; Hartlieb, M.; Sanchis, J.; Smith, T.; Perrier, S. Complex multiblock bottle-brush architectures by RAFT polymerization. *Chem. Commun.* **2017**, *53*, 11901–11904. [[CrossRef](#)]
19. Börner, H.G.; Duran, D.; Matyjaszewski, K.; Da Silva, M.; Sheiko, S.S. Synthesis of molecular brushes with gradient in grafting density by atom transfer polymerization. *Macromolecules* **2002**, *35*, 3387–3394. [[CrossRef](#)]
20. Liang, X.; Liu, Y.; Huang, J.; Wei, L.; Wang, G. Synthesis and characterization of novel barbwire-like graft polymers poly(ethylene oxide)-g-poly(-caprolactone)4 by the ‘grafting from’ strategy. *Polym. Chem.* **2015**, *6*, 466–475. [[CrossRef](#)]
21. Uhrig, D.; Mays, J.W. Synthesis of Combs, Centipedes, and Barbwires: thinspace Poly(isoprene-graft-styrene) Regular Multigraft Copolymers with Trifunctional, Tetrafunctional, and Hexafunctional Branch Points. *Macromolecules* **2002**, *35*, 7182–7190. [[CrossRef](#)]
22. Pelras, T.; Mahon, C.S.; Nonappa; Ikkala, O.; Gröschel, A.H.; Müllner, M. Polymer Nanowires with Highly Precise Internal Morphology and Topography. *J. Am. Chem. Soc.* **2018**, *140*, 12736–12740. [[CrossRef](#)] [[PubMed](#)]
23. Rosen, B.M.; Wilson, C.J.; Wilson, D.A.; Peterca, M.; Imam, M.R.; Percec, V. Dendron-mediated self-assembly, disassembly, and self-organization of complex systems. *Chem. Rev.* **2009**, *109*, 6275–6540. [[CrossRef](#)] [[PubMed](#)]
24. Evans, C.W.; Ho, D.; Marlow, J.B.; King, J.J.; Hee, C.; Wong, L.N.; Atkin, R.; Smith, N.M.; Warr, G.G.; Norret, M.; et al. Intracellular Communication between Synthetic Macromolecules. *JACS* **2022**, *144*, 14112–14120. [[CrossRef](#)]
25. Kröger M.; Peleg O.; Halperin A. From Dendrimers to Dendronized Polymers and Forests: Scaling Theory and its Limitations. *Macromolecules* **2010**, *43*, 6213–6224. [[CrossRef](#)]
26. Borisov, O.V.; Polotsky, A.A.; Rud, O.V.; Zhulina, E.B.; Leermakers, F.A.M.; Birshtein, T.M. Dendron Brushes and Dendronized Polymers: A Theoretical Outlook. *Soft Matter* **2014**, *10*, 2093–2101. [[CrossRef](#)]
27. Mikhailov, I.V.; Darinskii, A.A.; Zhulina, E.B.; Borisov, O.V.; Leermakers, F.A.M. Persistence length of dendronized polymers: The self-consistent field theory. *Soft Matter* **2015**, *11*, 9367–9378. [[CrossRef](#)]
28. Konak, C.; Reschel, T.; Oupicky, D.; Ulbrich, K. Thermally controlled association in aqueous solutions of poly(l-lysine) grafted with poly(N-isopropylacrylamide). *Langmuir* **2002**, *18*, 8217–8222. [[CrossRef](#)]
29. Jiang, X.; Lu, G.; Feng, C.; Li, Y.; Huang, X. Poly(acrylic acid)-graft-poly(N-vinylcaprolactam): A novel pH and thermo dual-stimuli responsive system. *Polym. Chem.* **2013**, *4*, 3876–3884. [[CrossRef](#)]
30. Zhang, D.; Dashtimoghadam, E.; Fahimipour, F.; Hu, X.; Li, Q.; Bersenev, E.A.; Ivanov, D.A.; Vatankhah-Varnosfaderani, M.; Sheiko, S.S. Tissue-adaptive materials with independently regulated modulus and transition temperature. *Adv. Mater.* **2020**, *32*, 2005314. [[CrossRef](#)]
31. Vashahi, F.; Martinez, M.R.; Dashtimoghadam, E.; Fahimipour, F.; Keith, A.N.; Bersenev, E.A.; Ivanov, D.A.; Zhulina, E.B.; Popryadukhin, P.; Matyjaszewski, K.; et al. Injectable bottlebrush hydrogels with tissue-mimetic mechanical properties. *Sci. Adv.* **2022**, *8*, eabm2469. [[CrossRef](#)]

32. Borisov O.V.; Zhulina E.B. Amphiphilic Graft Copolymers in a Selective Solvent: Intramolecular Structures and Conformational Transitions. *Macromolecules* **2005**, *38*, 2506–2514. [[CrossRef](#)]
33. Kosovan, P.; Kuldova, J.; Limpouchova, Z.; Prochazka, K.; Zhulina, E.B.; Borisov, O.V. Amphiphilic Graft Copolymers in Selective Solvents: Molecular Dynamics Simulations and Scaling Theory. *Macromolecules* **2009**, *42*, 6748–6760. [[CrossRef](#)]
34. Prokacheva, V.M.; Rud, O.V.; Uhlik, F.; Borisov, O.V. Intramolecular micellization and nanopatterning in pH-and thermo-responsive molecular brushes. *Soft Matter* **2020**, *16*, 208–218. [[CrossRef](#)]
35. Borisov, O.V.; Shavykin O.V.; Zhulina, E.B. Theory of polyelectrolyte dendrigrafts. *Colloid Polym. Sci.* **2020**, *298*, 951–959. [[CrossRef](#)]
36. Birshtein, T.M.; Borisov, O.V.; Zhulina, Y.B.; Khokhlov, A.R.; Yurasova, T.A. Conformations of comb-like macromolecules. *Polym. Sci. USSR* **1987**, *29*, 1293–1300. [[CrossRef](#)]
37. Fredrickson, G.H. Surfactant-induced lyotropic behavior of flexible polymer solutions. *Macromolecules* **1993**, *26*, 2825–2831. [[CrossRef](#)]
38. Borisov, O.V.; Birshtein, T.M.; Zhulina, Y.B. Temperature-Concentration Diagram of State for Solutions of Comb-like Macromolecules *Polym. Sci. USSR* **1987** *29*, 1552–1559. [[CrossRef](#)]
39. Zhulina, E.B.; Sheiko, S.S.; Borisov, O.V. Solution and Melts of Barbwire Bottlebrushes: Hierarchical Structure and Scale-Dependent Elasticity. *Macromolecules* **2019**, *52*, 1671–1684. [[CrossRef](#)]
40. Sheiko S.S.; Borisov O.V.; Prokhorova S.A.; Möller M. Cylindrical molecular brushes under poor solvent conditions: Microscopic observations and scaling analysis. *Eur. Phys. J. E* **2004**, *13*, 125–131. [[CrossRef](#)]
41. Subbotin, A.V.; Semenov, A.N. Spatial Self-Organization of Comb Macromolecules. *Polym. Sci. Ser. A* **2007**, *49*, 1328–1357. [[CrossRef](#)]
42. Zhulina, E.B.; Sheiko, S.S.; Borisov, O.V. Theoretical advances on molecular bottlebrushes: Solutions, gels, and self-assembly. *Soft Matter* **2022**, *18*, 8714–8732. [[CrossRef](#)]
43. Feuz, L.; Leermakers, F.A.M.; Textor, M.; Borisov, O. Bending rigidity and induced persistence length of molecular bottle brushes: A self-consistent-field theory. *Macromolecules* **2005**, *38*, 8891–8901. [[CrossRef](#)]
44. MSAariaho; Ikkala, O.; Szleifer, I.; Erukhimovich, I.; ten Brinke, G. On lyotropic behavior of molecular bottle-brushes: A Monte Carlo computer simulation study. *J. Chem. Phys.* **1997**, *107*, 3267–3276. [[CrossRef](#)]
45. Saariaho, M.; Szleifer, I.; Ikkala, O.; ten Brinke, G. Extended conformations of isolated molecular bottle-brushes: Influence of side-chain topology. *Macromol. Theor. Simul.* **1998**, *7*, 211–216. [[CrossRef](#)]
46. Subbotin, A.; Saariaho, M.; Ikkala, O.; ten Brinke, G. Elasticity of comb copolymer cylindrical brushes. *Macromolecules* **2000**, *33*, 3447–3452. [[CrossRef](#)]
47. Elli, S.; Ganazzoli, F.; Timoshenko, E.G.; Kuznetsov, Y.A.; Connolly, R. Size and persistence length of molecular bottle-brushes by Monte Carlo simulations. *J. Chem. Phys.* **2004**, *120*, 6257–6267. [[CrossRef](#)]
48. Theodorakis, P.E.; Hsu, H.-P.; Paul, W.; Binder, K. Computer simulation of bottle-brush polymers with flexible backbone: Good solvent versus theta solvent conditions. *J. Chem. Phys.* **2011**, *135*, 164903. [[CrossRef](#)]
49. Cao, Z.; Carrillo, J.-M.Y.; Sheiko, S.S.; Dobrynin, A.V. Computer Simulations of Bottle Brushes: From Melts to Soft Networks. *Macromolecules* **2015**, *48*, 5006–5015 [[CrossRef](#)]
50. Hsu, H.-P.; Paul, W.; Binder, K. One- and Two-Component Bottle-Brush Polymers: Simulations Compared to Theoretical Predictions. *Macromol. Theory Simul.* **2007**, *16*, 660–689. [[CrossRef](#)]
51. Hsu, H.-P.; Paul, W.; Binder, K. Standard definitions of persistence length do not describe the local intrinsic stiffness of real polymer chains. *Macromolecules* **2010**, *43*, 3094–3102. [[CrossRef](#)]
52. Hsu, H.-P.; Paul, W.; Binder, K. Estimation of persistence lengths of semiflexible polymers: Insight from simulations. *Polym. Sci. Ser. C* **2013**, *55*, 39–59. [[CrossRef](#)]
53. Muhammadi, E.; Joshi, S.J.; Deshmukh, S.A. Review of computational studies of bottlebrush polymers. *Computational Materials Science* **2021**, *199*, 110720 [[CrossRef](#)]
54. Zamurovic, M.; Christodoulou, S.; Vazaios, A.; Iatrou, E.; Pitsikalis, M.; Hadjichristidis, N. Micellization Behavior of Complex Comblike Block Copolymer Architectures. *Macromolecules* **2007**, *40*, 5835–5849. [[CrossRef](#)]
55. Li, Z.; Ma, J.; Xheng, C.; Zhang, K.; Wooley, K.L. Synthesis of Hetero-Grafted Amphiphilic Diblock Molecular Brushes and Their Self-Assembly in Aqueous Medium. *Macromolecules* **2010**, *43*, 1182–1184. [[CrossRef](#)]
56. Fenyves, R.; Schmutz, M.; Horner, I.J.; Bright, F.V.; Rzaev, J. Aqueous Self-Assembly of Giant Bottlebrush Block Copolymer Sufactants as Shape-Tunable Building Blocks. *J.Am.Chem.Soc.* **2014**, *136*, 7762–7770. [[CrossRef](#)]
57. Alaboalirat, M.; Qi, L.; Arrington, K.J.; Qian, S.; Keum, J.K.; Mei, H.; Littrell, K.C.; Sumpter, B.G.; Carrillo, J.-M.Y.; Verduzco, R.; et al. Amphiphilic Bottlebrush Block Copolymers: Analysis of Aqueous Self-Assembly by Small-Angle Neutron Scattering and Surface Tension Measurements. *Macromolecules* **2019**, *52*, 465–476. [[CrossRef](#)]
58. Kim, S.; Cho, Y.; Kim, J.H.; Song, S.; Lim, J.; Choi, S.-H.; Char, K. Structural Analysis of Bottlebrush Block Copolymer Micelles Using Small-angle X-ray Scattering. *ACS Macro Lett.* **2020**, *9*, 1261–1266. [[CrossRef](#)]
59. Taipaleenmaki, E.; Mouritzen, S.A.; Schattling, P.; Zhang, Y.; Städler, B. Mucopenetrating micelles with a PEG corona. *Nanoscale* **2017**, *9*, 18438–18448. [[CrossRef](#)]
60. Wang, Y.; Shao, F.; Sauve, E.R.; Tonge, C.M.; Hudson, Z.M. Self-assembly of giant bottlebrush block copolymer surfactants from luminescent organic electronic materials. *Soft Matter* **2019**, *15*, 5421–5430. [[CrossRef](#)]

61. Unsal, H.; Onbulak, S.; Calik, F.; Er-Rafik, M.; Schmutz, M.; Sanyal, A.; Rzayev, J. Interplay between Molecular Packing, Drug Loading, and Core Cross-Linking in Bottlebrush Copolymer Micelles. *Macromolecules* **2017**, *50*, 1342–1352. [[CrossRef](#)]
62. Patel, B.B.; Pan, T.; Chang, Y.; Walsha, D.J.; Kwok, J.J.; Parka, K.S.; Patela, K.; Guironnet, D.; Singa, C.E.; Diao, Y. Concentration-Driven Self-Assembly of PS-*b*-PLA Bottlebrush Diblock Copolymers in Solution. *ACS Polym. Au* **2022**, *2*, 232–244 [[CrossRef](#)] [[PubMed](#)]
63. Shibuya, Y.; Nguyen, H.V.T.; Johnson, J.A. Mikto-Brush-Arm Star Polymers via Cross-Linking of Dissimilar Bottlebrushes: Synthesis and Solution Morphologies. *ACS Macro Lett.* **2017**, *6*, 963–968. [[CrossRef](#)] [[PubMed](#)]
64. Henn, D.M.; Holmes, J.A.; Kent, E.W.; Zhao, B. Worm-to-Sphere Shape Transition of Thermoresponsive Linear Molecular Bottlebrushes in Moderately Concentrated Aqueous Solution. *J. Phys. Chem. B* **2018**, *122*, 7015–7025. [[CrossRef](#)] [[PubMed](#)]
65. Zhulina, E.B.; Borisov, O.V. Micelles Formed by AB Copolymer with Bottlebrush blocks. Scaling Theory. *J. Phys. Chem. B* **2021**, *125*, 12603–12616. [[CrossRef](#)] [[PubMed](#)]
66. Lebedeva, I.O.; Zhulina, E.B.; Borisov, O.V. Self-assembly of bottlebrush block copolymers in selective solvent: Micellar structures. *Polymers* **2021**, *13*, 1351. [[CrossRef](#)]
67. De Gennes, P.-G. *Scaling Concepts in Polymer Physics*; Cornell University Press: Ithaca, NY, USA; London, UK, 1979.
68. Duane, S.; Kennedy, A.D.; Pendleton, B.J.; Roweth, D. Hybrid Monte-Carlo. *Phys. Lett. B* **1987**, *195*, 216–222 [[CrossRef](#)]
69. Metropolis, N.; Rosenbluth, A.W.; Rosenbluth, M.N. Teller, A.H.; Teller, E. Equation of State Calculations by Fast Computing Machines. *J. Chem. Phys.* **1953**, *21*, 1087–1092 [[CrossRef](#)]
70. Irback, A. Hybrid Monte Carlo simulation of polymer chains. *J. Chem. Phys.* **1994**, *101*, 1661–1667 [[CrossRef](#)]
71. Grest, G.S.; Kremer, K. Molecular-Dynamics Simulation for Polymers in the Presence of a Heat Bath. *Phys. Rev. A* **1986**, *33*, 3628–3631 [[CrossRef](#)]
72. Jones, J.E. On the determination of molecular fields. I. From the variation of the viscosity of a gas with temperature. *Proc. R. Soc. London. Ser. A* **1924**, *106*, 441–462
73. Behbahani, A.F.; Schneider, L.; Rissanou, A.; Chazirakis, A.; Bacova, P.; Jana, P.K.; Li, W.; Doxastakis, M.; Polinska, P.; Burkhart, C.; et al. Dynamics and Rheology of Polymer Melts via Hierarchical Atomistic, Coarse-Grained, and Slip-Spring Simulations. *Macromolecules* **2021**, *54*, 2740–2762 [[CrossRef](#)]
74. McDonald, I.R. NPT-ensemble Monte Carlo calculations for binary liquid mixtures. *Mol. Phys.* **1971**, *23*, 41–58 [[CrossRef](#)]
75. Flyvbjerg, H.; Petersen, H.G. Error-Estimates on Averages of Correlated Data. *J. Chem. Phys.* **1989**, *91*, 461–466 [[CrossRef](#)]
76. Jin, S.; Collins, L.R. Dynamics of dissolved polymer chains in isotropic turbulence. *New J. Phys.* **2007**, *9*, 360 [[CrossRef](#)]